Diagnostic Study

INTERNATIONAL JOURNAL OF SURGERY

OPEN

MRI-based deep learning and radiomics for prediction of occult cervical lymph node metastasis and prognosis in early-stage oral and oropharyngeal squamous cell carcinoma: a diagnostic study

Tianjun Lan, PhD[a,b], Shijia Kuang, MD[a,b], Peisheng Liang, PhD[c], Chenglin Ning, MCs[d], Qunxing Li, PhD[a,b], Liansheng Wang, MD[a,b], Youyuan Wang, PhD[a,b], Zhaoyu Lin, PhD[a,b], Huijun Hu, MD[e], Lingjie Yang, MD[e], Jintao Li, MD[a,b], Jingkang Liu, MD[a,b], Yanyan Li, MD[a,b], Fan Wu, PhD[a,b], Hua Chai, PhD[f], Xinpeng Song, BSc[f], Yiqian Huang, BSc[f], Xiaohui Duan, PhD[e,*], Dong Zeng[d,g,*], Jinsong Li, PhD[a,b,*], Haotian Cao, MD, PhD[a,b,*]

Introduction: The incidence of occult cervical lymph node metastases (OCLNM) is reported to be 20–30% in early-stage oral cancer and oropharyngeal cancer. There is a lack of an accurate diagnostic method to predict occult lymph node metastasis and to help surgeons make precise treatment decisions.

Aim: To construct and evaluate a preoperative diagnostic method to predict OCLNM in early-stage oral and oropharyngeal squamous cell carcinoma (OC and OP SCC) based on deep learning features (DLFs) and radiomics features.

Methods: A total of 319 patients diagnosed with early-stage OC or OP SCC were retrospectively enrolled and divided into training, test and external validation sets. Traditional radiomics features and DLFs were extracted from their MRI images. The least absolute shrinkage and selection operator (LASSO) analysis was employed to identify the most valuable features. Prediction models for OCLNM were developed using radiomics features and DLFs. The effectiveness of the models and their clinical applicability were evaluated using the area under the curve (AUC), decision curve analysis (DCA), and survival analysis.

Results: Seventeen prediction models were constructed. The Resnet50 deep learning (DL) model based on the combination of radiomics and DL features achieves the optimal performance, with AUC values of 0.928 (95% CI: 0.881–0.975), 0.878 (95% CI: 0.766–0.990), 0.796 (95% CI: 0.666–0.927), and 0.834 (95% CI: 0.721–0.947) in the training, test, external validation set1, and external validation set2, respectively. Moreover, the Resnet50 model has great prediction value of prognosis in patients with early-stage OC and OP SCC.

Conclusion: The proposed MRI-based Resnet50 DL model demonstrated high capability in diagnosis of OCLNM and prognosis prediction in the early-stage OC and OP SCC. The Resnet50 model could help refine the clinical diagnosis and treatment of the early-stage OC and OP SCC.

Keywords: deep learning, MRI, occult cervical lymph node metastasis, oral and oropharyngeal squamous cell carcinoma, radiomics

[a]Department of Oral and Maxillofacial Surgery, Sun Yat-Sen Memorial Hospital, Sun Yat-Sen University, Guangzhou, [b]Guangdong Provincial Key Laboratory of Malignant Tumor Epigenetics and Gene Regulation, Guangdong-Hong Kong Joint Laboratory for RNA Medicine, Medical Research Center, Sun Yat-Sen Memorial Hospital, Guangzhou, [c]Guanghua School of Stomatology, Hospital of Stomatology, Guangdong Province Key Laboratory of Stomatology, Sun Yat-Sen University, Guangzhou, [d]School of Biomedical Engineering, Southern Medical University, Guangzhou, [e]Department of Radiology, Sun Yat-Sen Memorial Hospital, Sun Yat-Sen University, Guangzhou, [f]School of Mathematics and Big Data, Foshan University, Foshan, Guangdong and [g]Department of Radiology, Zhujiang Hospital, Southern Medical University, Guangzhou, Guangdong, People's Republic of China

Tianjun Lan, Shijia Kuang, Peisheng Liang, and Chenglin Ning contributed equally to this work.

Sponsorships or competing interests that may be relevant to content are disclosed at the end of this article.

**Corresponding authors. Address: Department of Oral and Maxillofacial Surgery, Sun Yat-Sen Memorial Hospital, Sun Yat-Sen University, Guangzhou 510120, Guangdong, People's Republic of China. Tel.: + 861 992 763 1809. E-mail: caobleat@hotmail.com (H. Cao), and Tel.: + 861 360 900 1967. E-mail: ljins@mail.sysu.edu.cn (J. Li); School of Biomedical Engineering, Southern Medical University, Guangdong 510515, Guangdong, People's Republic of China. Tel.: + 861 562 643 9092. E-mail: zd1989@smu.edu.cn (D. Zeng); Department of Radiology, Sun Yat-Sen Memorial Hospital, Sun Yat-Sen University, Guangzhou 510120, Guangdong, People's Republic of China. Tel.: + 861 351 276 2365. E-mail: duanxh5@mail.sysu.edu.cn (X. Duan).*

International Journal of Surgery (2024) 110:4648–4659

Received 21 December 2023; Accepted 25 April 2024

Published online 9 May 2024

http://dx.doi.org/10.1097/JS9.0000000000001578

Introduction

Oral and oropharyngeal squamous cell carcinoma (OC and OP SCC) are the most prevalent malignant head and neck cancers. They account for more than 300 000 new cases and cause over 200 000 deaths globally each year[1]. The primary risk factors for OC and OP SCC include alcohol using, smoking, infection with human papillomavirus, extranodal extension, positive surgical margins, perineural invasion, vascular invasion, and lymph node metastasis (LNM)[2]. In particular, occult cervical lymph node metastases (OCLNM) is one of the most important prognostic factors for patients with early-stage OC and OP SCC[3]. OCLNM, defined as clinically undetected metastases during diagnostic work before treatment, was associated with tumor recurrence and decreased survival in early-stage OC and OP SCC[3]. For patients with early-stage OC and OP SCC, the incidence of OCLNM is reported to be 20–30%[3–5]. Blind neck dissection may result in overtreatment in 70–80% of patients, which can cause functional impairment, reduction in quality of life, and even death[5]. There remains a debate on whether patients with early-stage OC and OP SCC should routinely undergo neck dissection. Therefore, accurately identifying LNM status is critical for therapeutic control and management of early-stage OC and OP SCC.

Depth of invasion (DOI), extranodal extension, tumor-stroma ratio, tumor budding, and tumor-infiltrating lymphocytes have been reported to be associated with the OCLNM[6–10]. However, the evaluation of these factors requires postoperative pathological examination. Recently, sentinel lymph node biopsy (SLNB) has demonstrated good performance in preoperative diagnosis of OCLNM[11]. However, due to the high rate of false positivity, there remains controversial for using SLNB to stage early-stage patients with oral squamous cell carcinoma for elective neck dissection (END)[11]. Currently, the diagnosis of OCLNM depends on preoperative imaging examination, such as MRI, X-ray computed tomography (CT), positron emission tomography (PET), and ultrasonography (US). Because MRI, CT, and US mainly focus on the morphological features of lymph nodes, including their size, heterogeneity and necrosis, it is not specific to detect metastatic lymph nodes[12–15]. As for PET-CT, false negativity may occur when the nodal lesions are small or contain cancer cell deposit[12,16]. Thus, there is currently a lack of an accurate diagnostic method to predict occult LNM and to help surgeons make precise treatment decisions.

Recently, there is an increased interest in using radiomics to improve clinical diagnosis and treatment. Radiomics applies improved image analysis by high-throughput extraction of large amounts of features from radiographic images[17]. Through the process of radiomics, quantitative features can be extracted from medical images[18,19]. These quantitative imaging features could potentially be used as prognostic or predictive biomarkers to improve predictive accuracy in medical field[20]. Despite its potential, radiomics can be affected by variations in image acquisition, reconstruction protocols, and preprocessing manipulation[21–23]. These variations can impact the robustness and scalability of radiomics models[23]. Deep learning (DL) has shown superior capabilities over traditional radiomics models in areas such as image classification, object detection, and segmentation[24,25]. It has the ability to learn intricate patterns from medical images and effectively apply them to new data, significantly enhancing the accuracy, efficiency, and consistency of medical imaging analysis[25,26]. MRI-based radiomics signature of the primary tumor has attained the ability to predict OCLNM, tumor stage, prognosis and drug response in OSCC[27,28]. However, these previous reports only focus on radiomics features and clinical factors, excluding the deep learning features (DLF), which contain valuable information. So far, there is no literature available on combined radiomics features and DLF for analyzing OCLNM in patients with early-stage OC and OP SCC.

In this study, we develop and validate the noninvasively preoperative prediction models of OCLNM based on radiomics features and DLF from two cohorts of early-stage OC and OP SCC. Then, we explore the role of our model in prognosis prediction.

HIGHLIGHTS

- A novel MRI-based Resnet50 deep learning model developed to predict occult lymph node metastasis in early-stage oral and oropharyngeal squamous cell carcinoma.
- The Resnet50 DL model have a good performance with area under the curve values of 0.9177 (95% CI: 0.8628–0.9725), 0.85 (95% CI: 0.7237–0.9763), and 0.7205 (95% CI: 0.5822–0.8588) in the training, test and external validation set, respectively.

Method

Ethnic and registration

This study was approved by the Ethics Committee of Hospital of Stomatology, Sun Yat-sen University (ERC-[2017]-30) and the Institutional Review Board of Sun Yat-sen Memorial Hospital, Sun Yat-sen University (No.SYSKY-2023-426-01). The registration number is NCT06366906 on clinicaltrails.org. The study was undertaken according to the Strengthening the Reporting of Observational Studies in Epidemiology (STROBE) guidelines and in accordance with the latest version of the Declaration of Helsinki[29]. The work has been reported in line with the STARD (Standards for the Reporting of Diagnostic accuracy studies) criteria[30].

Study population

To find out the radiomics features that affects the prediction of OCLNM in OC and OP SCC. A total of 319 patients with early-stage OC or OP SCC from two hospitals [Hospital of Stomatology of Sun Yat-sen University (Cohort A, $n = 121$) and Sun Yat-sen Memorial Hospital (Cohort B, $n = 198$)], were retrospectively retrieved from 1 January 2017 to 30 December 2022. This study was approved by the institutional review board of both participating institutions. Due to the retrospective and deidentified data utilized in the study, the informed consent was waived. Data use agreements were established, if applicable, between the Hospital of Stomatology of Sun Yat-sen University and the Sun Yat-sen Memorial Hospital. Inclusion criteria were as follows: (1) Pathologically confirmed, previously untreated oral and oropharyngeal squamous cell carcinoma with radical resection; (2) MRI examination was performed 2 weeks before surgery; (3) All patients with neck dissection and the status of

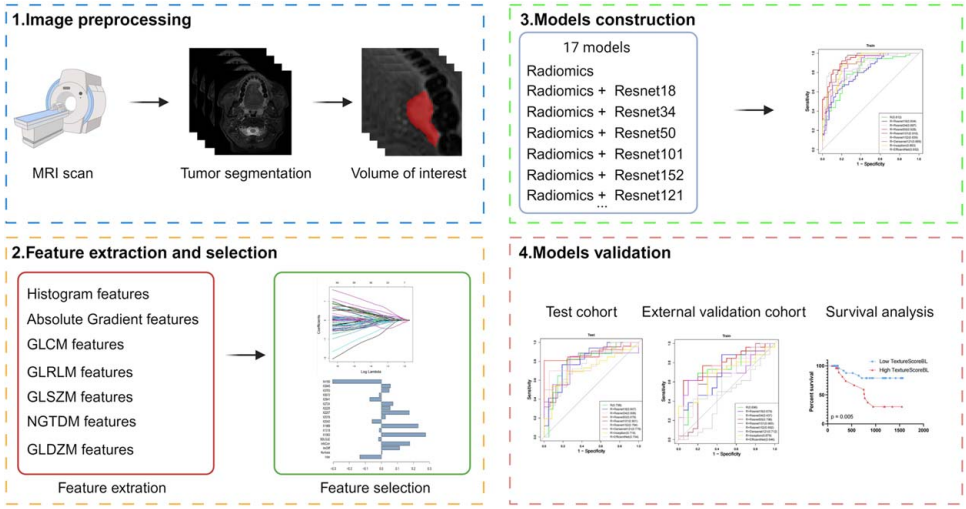

Figure 1. The flow chart of the method. First, ROIs of the primary tumor segmented on T1-weighted and T2-weighted images. Then, these ROIs were applied to three-dimensionally reconstruct primary tumor. And the three-dimensional radiomics features and deep learning features were extracted for further analysis. Next, based on above features, 17 predictive models were constructed in this study. Finally, an optimal predictive model was selected to predict OCLNM via models compared and validation.

regional lymph nodes was confirmed via pathological examination; (4) All patients had no clinical evidence of nodal involvement. Exclusion criteria were as follows: (1) Other malignant tumor, such as adenoid cystic carcinoma; (2) a lack of complete MRI imaging or poor MRI imaging quality; (3) patients had undergone neck dissection or treated nonsurgically; (4) patients with metastatic disease.

In this study, the Cohort A was randomly divided as the training and test sets in a 7:3 ratio, and the Cohort B was segmented into two groups based on the batched collected, which were defined as external validation set1 ($n = 68$) and external validation set2 ($n = 130$).

MRI preprocessing

The MRI examinations of Cohort A were conducted using a Philips 1.5T Achieva superconducting MR scanner (Philips Healthcare, Best, the Netherlands), encompassing the region from the skull base down to the clavicle level. The contrast-enhanced T1-weighted imaging (ce-T1WI) sequence and the T2-weighted imaging (T2WI) sequence was applied to further analysis. The image acquisition parameters were as follows: ceT1WI repetition/echo time, 574/9.9 ms; T2WI repetition/echo time, 4970/96 ms; matrix, 224×320; field of view, 246×246 mm^2; slice thickness, 5 mm; and gap between slices, 1.5 mm. The MRI examinations of external validation set1 from Cohort B were conducted using a Philips 1.5T Achieva superconducting MR scanner (Philips Healthcare, Best). The image acquisition parameters were as follows: ceT1WI repetition/echo time, 510–600/12–16 ms; T2WI repetition/echo time, 3500–4000/80–90 ms; matrix, 256–288 × 192–268; field of view, 230–250 × 230–250 mm^2; slice thickness, 4 mm; and gap between slices, 0.4–1 mm. The MRI examinations of external validation set2 from Cohort B were conducted using a Siemens 1.5T AVANTO superconducting MR scanner (Siemens Healthineers). The image acquisition parameters were as follows: ceT1WI repetition/echo time, 500–600/8–12 ms; T2WI repetition/echo time, 2500–3500/90–100 ms; matrix, 256–288 × 208–268; field of view, 240–250 × 240–250 mm^2; slice thickness, 4 mm; and gap between slices, 0.4–1 mm. The linear interpolation was applied to reduce the difference from scanning devices and processes among patients. The pixel spacing and slice spacing were set to 0.6 mm and 4.0 mm, respectively. To acquire high-quality images, the voxel intensity of each scan was normalized, ensuring a mean of 0.0 and a SD of 1.0 for the voxel intensities. The flow chart of the method was shown in Figure 1.

Segmentation of tumor images

The primary tumor areas were outlined and segmented from MRI images to generate the corresponding interested region of interest (ROI) slice-by-slice by an expert oral-maxillofacial radiologist (with 10 years of experience in oral-maxillofacial MRI interpretation), who was blinded to outcomes, using ITK-SNAP software (www.itk-snap.org). The MRI image of the primary tumor and the corresponding segmentation results were showed in Figure 2.

Radiomics features extraction

Based on the Image Biomarker Standardization Initiative (IBSI), we extracted a total of 94 features on T1 and T2 images via traditional radiomics, including first-order features such as median, mean, minimum, maximum, SD, skewness, and kurtosis, as well as higher-order features like the Gray Level Co-occurrence Matrix (GLCM), Gray Level Run-Length Matrix (GLRLM), Gray Level Size Zone Matrix (GLSZM), Neighbouring Gray Tone Difference Matrix (NGTDM), Neighboring grey level dependence Matrix (NGLDM), and Grey Level Distant Zone Matrix (GLDZM), with the bin size for higher-order features set to 128 and using the Linear method for image and ROI resampling. All features were extracted via the Standardized Environment for Radiomics Analysis (SERA) Package using MatlabR2019b.

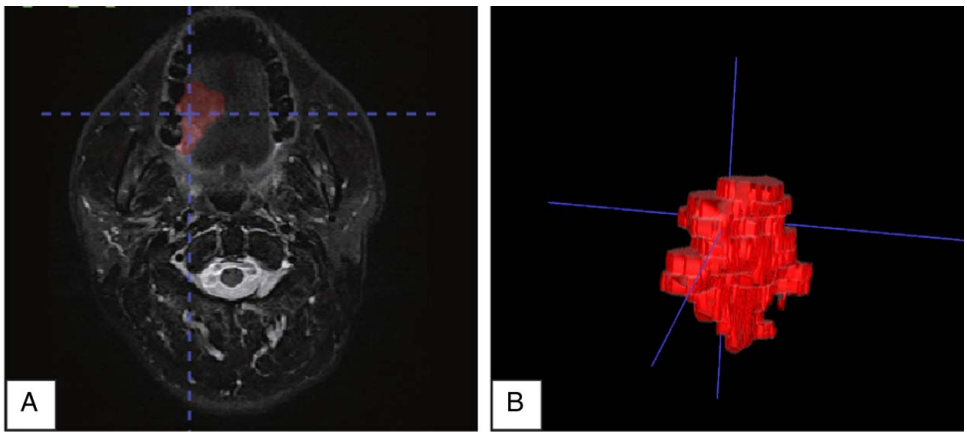

Figure 2. Tumor segmentation. A. The MRI image was marked manually for the tumor; B. The three-dimensionally reconstructed tumor.

Deep learning features extraction and fusion

To overcome the problem of traditional radiomics features, we also extracted DLF for fusion with radiomics. Before extracting DLF, the data is processed with the following steps: (1) Select the mask with the largest ROI area in the labeled MRI, and combine the upper and lower image of it as the three-channel input image of the DL model; (2) Crop MRI images using minimal circumscribed rectangles; (3) resize the tumor patch to 224×224 pixels.

We used eight convolutional neural networks (CNNs), including Resnet-18, Resnet-34, Resnet-50, Resnet-101, Resnet-152, Densenet-121, Inception, and EfficientNet. These CNNs have powerful feature extraction capabilities, and their encoder serve as the output of DLF. All CNNs were pretrained with ImageNet, which is a dataset of millions of images and a thousand categories that can help extract features better.

Based on these pretrained networks, we extracted 512, 512, 2048, 2048, 2048, 1024, 2048, and 1280 features from the T1 and T2 images (Fig. 3).

Data processing

After fusing the features of different CNNs with the radiomics features, we normalized all features with a Z-score method and eliminated the features with constant values. Considering the insufficient samples in the training set and the imbalance of data categories (42/47), we used the SMOTE (Synthetic Minority Over-sampling) method to simplify a few categories to increase the number of samples in the training set and adjust the balance of data categories. For the external validation set, normalization was performed using the mean and variance derived from the training set, and any features identical to those in the training set were excluded.

Feature selection

To prevent overfitting, we took a two-step feature selection method to select the best feature to distinguish cervical LNM. The Spearman correlation test was first used to assess the linear correlation between the features, and when the Spearman correlation coefficient between the two features is > 0.9, we selected one of the features for subsequent analysis. Finally, the least absolute shrinkage and selection operator (LASSO) regression was used for feature selection, with nonzero coefficients as valuable predictors in each feature group.

Model construction

After feature selecting, we used a generalized regression linear model for machine learning classification in each ensemble feature group. To verify whether DLF can promote the judgment of LNM compared to radiomics features alone, we designed a multigroup comparison experiment that uses radiomics features singly to build predictive model and other models constructed based on radiomics features + DLF. The 10-fold cross-validation approach was applied to train these models in the training set. The area under the receiver operating characteristic (ROC) curve (AUC) and the accuracy (ACC) were used to quantitatively evaluate the performance of each model.

Model validation

In this study, the predictive capability of the above models was validated in the test set. Based on the AUC and ACC, the best prediction model was identified. To explore the robust of the selected model, we performed the ROC analysis in the external validation set. Moreover, we applied the Log-rank test to evaluate the prognostic value of the model.

Statistical analysis

The Z-score normalization in our study was completed on Matlab2019 (MathWorks, Natick, America); The Spearman correlation test and the LASSO regression analysis were performed on R-4.2.1, and the Delong test was performed on R-4.2.1 to test the difference between the models.

Result

Characteristic of patients

The characteristics of the study participants are shown in Table 1. In the present study, 319 patients were included, of which 207 (64.89%) were men and 112 (35.11%) were women. The study comprised two cohorts from two independent medical centers (the Hospital of Stomatology of Sun Yat-sen University [cohort A, $n = 121$] and the Sun Yat-sen Memorial Hospital [cohort B,

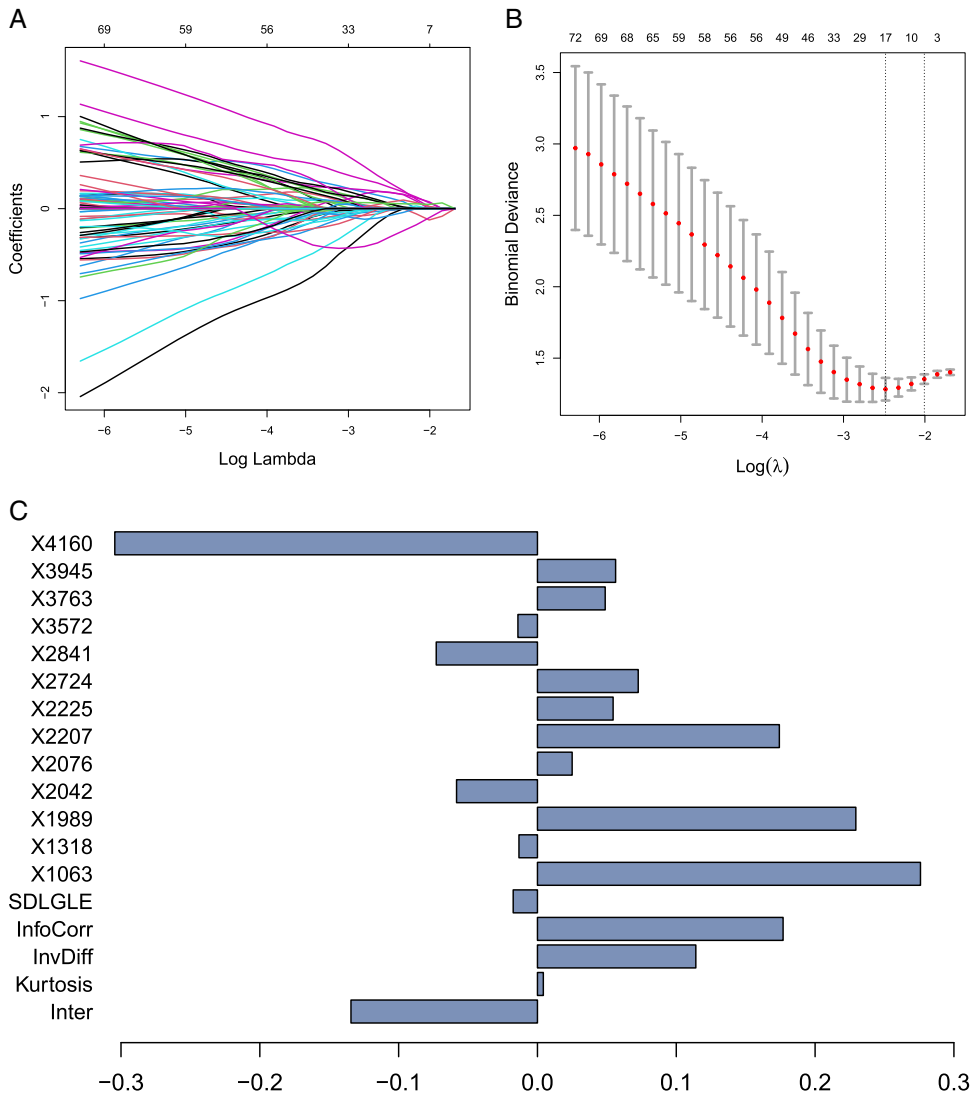

Figure 3. The feature selection from the combination of Radiomics and Resnet50. A. LASSO regression coefficient of the features. Different color line shows corresponding coefficient of each feature; B. Tuning parameter (λ) selection in LASSO model; C. Values of fusion features. InfoCorr, information theoretic correlation; InvDiff, inverse difference; Inter, intercept; SDLGLE, small distance low grey level emphasis; X, Deep learning features.

$n = 198$]). Among these patients, 125 patients were with T1 stage and 194 patients with T2 stage. Most patients suffered from oral cavity squamous cell carcinoma [250 of 319 (78.37%)]. A total of 163 patients (51.10%) had OCLNM. In the cohort B, a minimum of 1 years of clinical follow-up was available.

In the present study, we conducted univariate comparisons between two cohorts (Table 1). Our findings revealed no significant differences in gender, clinical T stage, and subsite (Table 1). This finding suggests that both cohorts had comparable clinical characteristics, thereby ensuring that no difference in distribution will influence the outcome of the predictive models.

Feature subset selection

In the present study, a small number of samples were sampled using the SMOTE method to appropriately increase the sample balance of the categories, which revealed 54 patients with LNM and 47 patients without nodal metastases. Then, we performed the Spearman correlation test and LASSO analysis to identify key features in the training set. Following the correlation test, we obtained 73 features from Radiomics, 824 from the combination of Radiomics and Resnet18, 727 from the combination of Radiomics and Resnet34, 1773 from the combination of Radiomics and Resnet50, 1499 from the combination of Radiomics and Resnet101, 1501 from the combination of Radiomics and Resnet152, 1369 from the combination of Radiomics and Densenet121, 4171 from the combination of Radiomics and Inception, and 2633 from the combination of Radiomics and EfficientNet. Next, LASSO analysis was applied for further feature reduction. Fifteen features from Radiomics, 17 features from Resnet-18, 7 features from Resnet-34, 5 features from Resnet-50, 5 features from Resnet-101, 7 features from Resnet-152, 10 features from Densenet-121, 12 features from

Table 1

Patient characteristics of the cohorts.

Characteristics	Cohort A	Cohort B	*P*
Total (*n* = count)	121	198	
Age (median, years)	51 (19–81)	57 (24–88)	< 0.001
Age group (%)			
18–44	30.58	20.20	0.047
45–64	54.55	51.52	
65–74	13.22	20.71	
≥ 75	1.65	7.58	
Sex (*n* = count)			
Male	80	127	0.720
Female	41	71	
Clinical T stage (*n* = count)			
T1	48	77	0.890
T2	73	121	
Subsite (*n* = count)			
Oral cavity	90	160	0.176
Oropharynx	31	38	
Node Status (*n* = count)			
Positive	70	86	0.012
Negative	51	112	
OS months (median, years)	–	210 (89–1714)	

Inception, 21 features from EfficientNet, 7 from the combination of Radiomics and Resnet18, 9 from the combination of Radiomics and Resnet34, 18 from the combination of Radiomics and Resnet50, 21 from the combination of Radiomics and Resnet101, 8 from the combination of Radiomics and Resnet152, 12 from the combination of Radiomics and Densenet121, 12 from the combination of Radiomics and Inception, and 9 from the combination of Radiomics and EfficientNet were obtained (Fig. 3). The process of feature selection in the combination of Radiomics and Resnet50 were shown in the Figures 3A and B. In the final 18 features screened via Radiomics and Resnet50, 5 features were traditional radiomics features and the rest 13 were DLF (Fig. 3C).

Model construction, comparison, and evaluation

The activation maps of features recognized and focused by the deep CNNs for LNM positive versus LNM negative early-stage OC and OP SCC were shown in Figure 4. Based on the above selected features, 17 predictive models were constructed in this study. To explore the impact of different DLF on the performance of models and confirm the optimal predictive model, we compared the capability of these models in the training set and the test set. As a result, the pretrained DL model Resnet50 combined with radiomics achieves the best performance, with the AUC of 0.928 (95% CI: 0.881–0.975), ACC of 0.861, and NPV of 0.860 in the training set (Table 2, Figs 5A, B). Consistent with that in the training set, Resnet50 combined with radiomics outperformed the other sixteen models in the test set, with AUC of 0.878 (95% CI: 0.766–0.990), ACC of 0.868, and NPV of 0.706 (Table 3, Figs 5C, D). To further evaluate the diagnostic accuracy for OCLNM, decision curve analysis (DCA) curves was applied (Fig. 5E). Among these models, Resnet50 showed the best net benefit rate. Moreover, we construct a nomogram based on the score results and classification results of the model built by Radiomics + Resnet50, which quantified the OCLNM predictions of early-stage OC and OP SCC (Figs 5F, G). By summing up the score for each independent predictor, we obtained the total

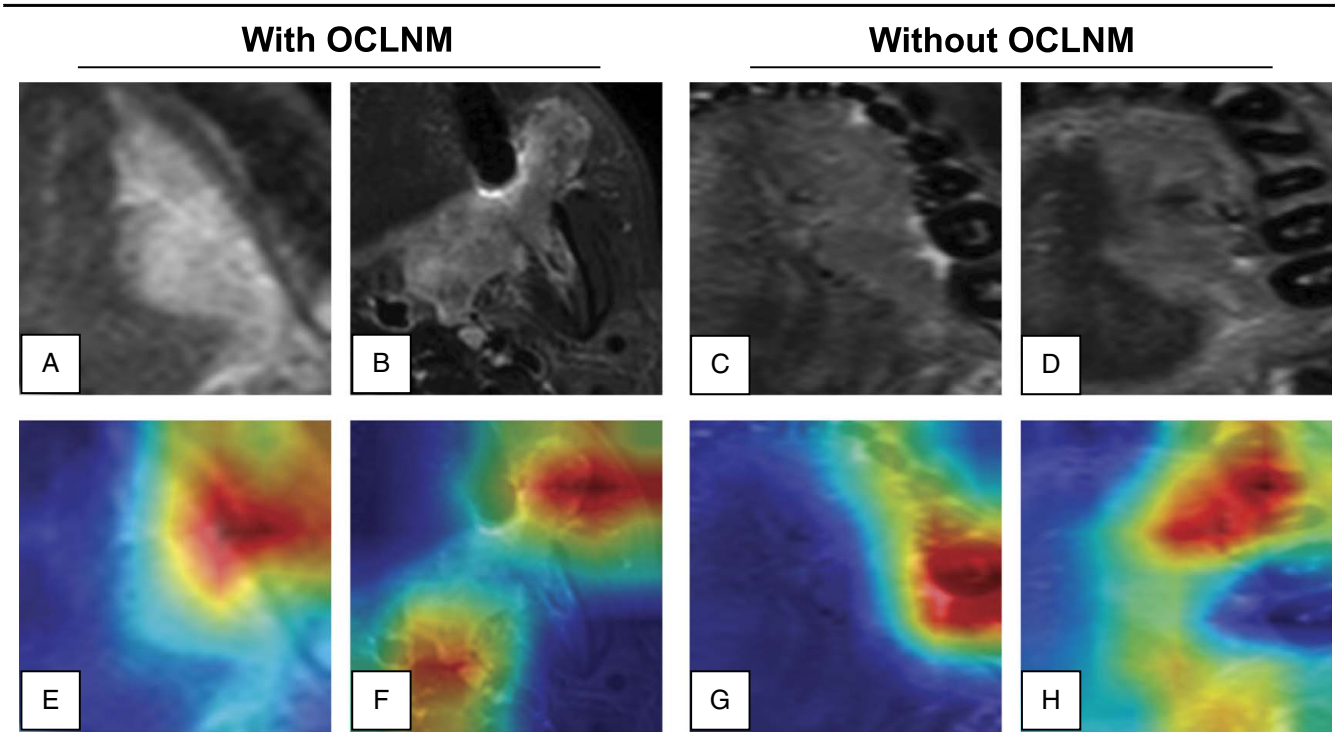

Figure 4. Activation maps of features recognized and focused by the deep convolutional neural networks for LNM positive versus LNM negative early-stage OC and OP SCC.

Table 2

The training results of different DL methods.

Experience	AUC	ACC	SPE	SEN	PPV	NPV	Delong (95% CI)
Radiomics	0.812	0.768	0.750	0.782	0.796	0.733	0.727–0.898
Resnet18	0.863	0.820	0.750	0.885	0.793	0.857	0.792–0.935
Resnet34	0.798	0.740	0.899	0.596	0.861	0.672	0.710–0.885
Resnet50	0.823	0.782	0.846	0.714	0.814	0.759	0.738–0.908
Resnet101	0.767	0.748	0.739	0.755	0.769	0.723	0.673–0.862
Resnet152	0.800	0.750	0.792	0.712	0.787	0.717	0.714–0.886
Densenet121	0.824	0.748	0.756	0.741	0.784	0.708	0.743–0.905
EfficientNet	0.932	0.871	0.942	0.796	0.929	0.831	0.884–0.980
Inception	0.920	0.842	0.868	0.813	0.848	0.836	0.870–0.970
Resnet18 + Radiomics	0.804	0.717	0.841	0.618	0.829	0.638	0.718–0.889
Resnet34 + Radiomics	0.887	0.859	0.933	0.796	0.935	0.792	0.818–0.956
Resnet50 + Radiomics	0.928	0.861	0.891	0.826	0.864	0.860	0.881–0.975
Resnet101 + Radiomics	0.918	0.860	0.800	0.920	0.821	0.909	0.864–0.971
Resnet152 + Radiomics	0.839	0.760	0.625	0.885	0.719	0.833	0.762–0.915
Densenet121 + Radiomics	0.869	0.804	0.737	0.889	0.727	0.894	0.802–0.937
EfficientNet + Radiomics	0.852	0.810	0.898	0.726	0.881	0.759	0.779–0.926
Inception + Radiomics	0.893	0.832	0.800	0.870	0.783	0.880	0.834–0.952

number of points, by which we estimated the occurrence of OCLNM for early-stage OC and OP SCC patients.

External validation and survival analysis

To evaluate the robust of the Resnet50 model, two external validation cohorts with follow-up data ($n = 197$) was applied in this study (Fig. 6A). The Resnet50 achieves stable performance in the external validation set1 and the external validation set2, with AUC of 0.796 (95% CI: 0.666–0.927), ACC of 0.761, and NPV of 0.655, and with AUC of 0.834 (95% CI: 0.721–0.947), ACC of 0.784, and NPV of 0.938, respectively (Table 4, Table 5, Figs 6A, B). Moreover, to evaluate the prognosis predictive value of the Resnet50 model for early-stage OC and OP SCC patients, the Kaplan–Meier survival curves was performed in the external validation set1 and the external validation set2, respectively (Figs 6C, D). In the two external validation sets, the patients with low radiomics score (≤ 0.033) had better prognosis than those with a high score (> 0.033) (Figs 6C, D). This indicates that Resnet50 has great prediction value for prognosis in patients with early-stage OC and OP SCC.

Discussion

Whether to perform cervical lymph node dissection for early-stage cancer and the type and scope of cervical lymph node dissection for locally advanced cancer are two of most important unsolved problems in oral and maxillofacial head and neck tumor surgery[31,32]. Although evidence suggests that prophylactic neck dissection may yield a higher 5-year survival rate (75 vs. 65%) compared to local extensive resection, clear guidelines on the necessity of neck dissection for early-stage cancers are still lacking[33]. The reason is that neck cleaning can cause head, neck, and shoulder dysfunction and damage immune function. There are also many controversies about whether to perform contralateral cervical lymph node dissection for midline tumors and locally advanced tumors. Sentinel lymph node detection has certain reference significance for the treatment of other cancer types. However, due to the particularity of lymphatic drainage in maxillofacial region, the accuracy of this method is poor[34]. Needle biopsy is of diagnostic significance in cases where LNM is suspected. However, lymph nodes with not obvious clinical symptoms cannot be punctures one by one. As such, a deeper and more precise prediction of the status of cervical lymph nodes is essential.

In the present study, several models based on preoperative MRI radiomic features and DLF were constructed and tested for prediction of OCLNM in early-stage OC and OP SCC. Among these prediction models, the DL model Resnet50 demonstrated superior diagnostic proficiency, as evidenced by its AUC values of 0.928, 0.878, 0.796, and 0.834, along with accuracy values of 0.861, 0.868, 0.761, and 0.784 for the training, test, external validation set1, and external validation set2, respectively. Moreover, Resnet50 demonstrated impressive ability for stratifying OS. Overall, the DL model Resnet50 showcased significant clinical advantages, suggesting its potential as a beneficial preoperative indicator for guiding clinical decisions.

Lymph node metastases (LNM) is a major risk factor for postsurgical tumor prognosis, and it determines the therapeutic outcomes of patients with oral and oropharyngeal squamous cell carcinoma[35,36]. LNM is vital in determining the treatment approach for patients with OC and OP SCC. Clinical palpation examination, a widely used noninvasive method for assessing lymph node status in clinical settings, is subjective and heavily reliant on the individual expertise of clinicians[37]. With the widespread use of imaging techniques such as CT, US, MRI, and PET-CT, the conventional standards of CT and MR morphology have been extensively utilized for assessing the cervical lymph node status in patients with OC and OP SCC[15,38,39]. Based on the current standards, lymph nodes exceeding 10 mm are deemed abnormal. However, nearly 20% of such lymph nodes are pathologically free of disease, and up to 23% patients exhibit histological extracapsule spread with lymph nodes of smaller than 10 mm[37]. This finding suggests that some patients may be subjected to overtreatment. Therefore, the diagnostic value of conventional MRI and CT is limited. Moreover, the measurement

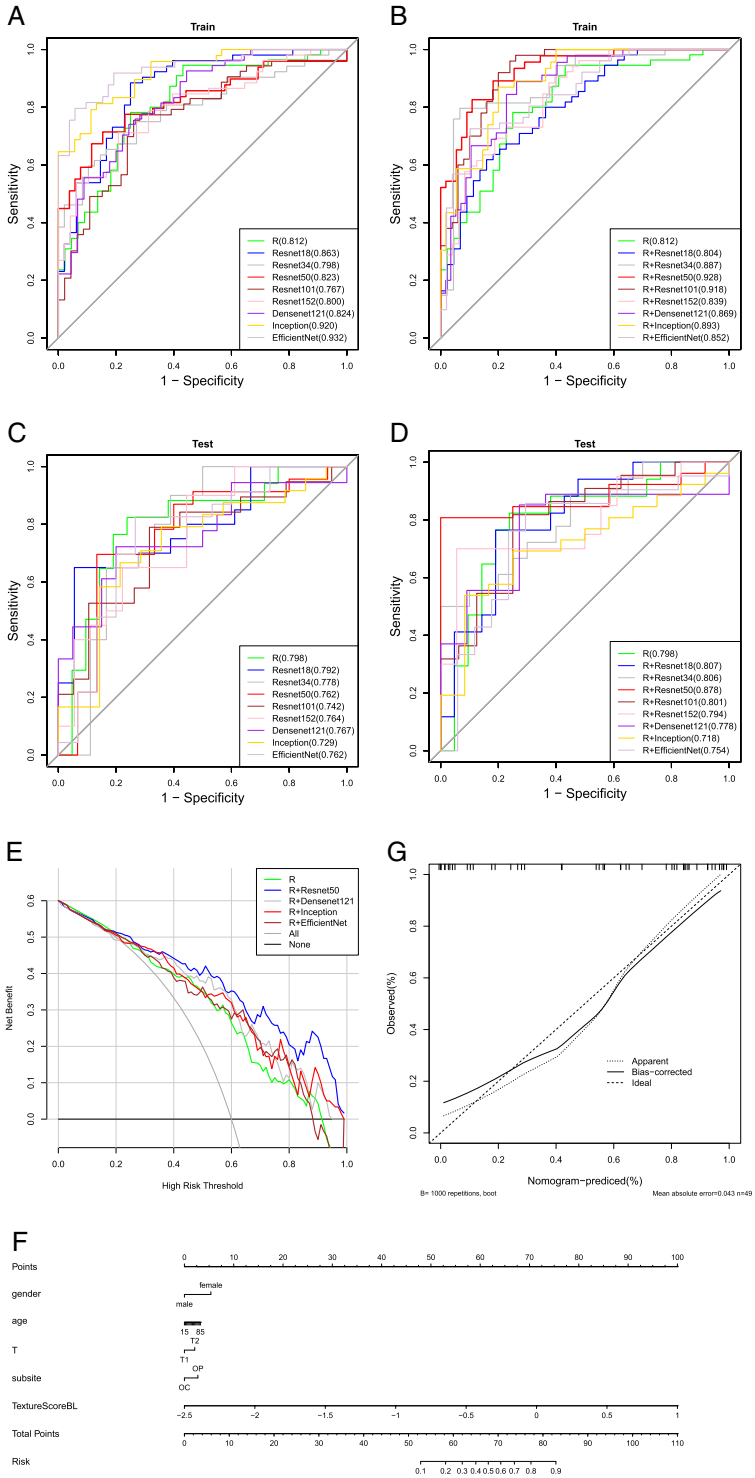

Figure 5. Construction and comparison of the models based on DLF and radiomics features. A. The ROC curves of prediction models based on radiomics features in the training set; B. The ROC curves of prediction models based on combined radiomics features and DLF in the training set; C. The ROC curves of prediction models based on radiomics features in the test set; D. The ROC curves of prediction models based on combined radiomics features and DLF in the test set; E. Decision curve analysis (DCA) of models; F. The predictive nomogram of OCLNM; G. Calibration curves of the predictive nomogram.

of tumor thickness or DOI was utilized to pinpoint the patients who would obtain the maximum benefit from END[40]. A patient with tumor DOI greater than 4 mm was strongly recommended for END[11]. However, its ability to differentiate is not as efficient as expected. To date, the gold standard remains the postoperative histopathological analysis on lymph nodes. As for micrometastasis, it can only be identified by surgical pathologists through a detailed examination of the excised specimen. The

Table 3

The testing results of different DL methods.

Experience	AUC	ACC	SPE	SEN	PPV	NPV	Delong (95% CI)
Radiomics	0.798	0.790	0.762	0.824	0.737	0.842	0.647–0.949
Resnet18	0.792	0.790	0.944	0.650	0.929	0.708	0.646–0.938
Resnet34	0.778	0.763	0.611	0.999	0.729	0.846	0.614–0.942
Resnet50	0.762	0.763	0.867	0.696	0.889	0.650	0.560–0.936
Resnet101	0.742	0.737	0.684	0.790	0.714	0.765	0.580–0.905
Resnet152	0.764	0.737	0.556	0.900	0.692	0.833	0.609–0.919
Densenet121	0.767	0.763	0.800	0.722	0.765	0.762	0.608–0.925
EfficientNet	0.762	0.790	0.733	0.826	0.826	0.733	0.592–0.933
Inception	0.729	0.711	0.786	0.667	0.842	0.579	0.554–0.904
Resnet18 + Radiomics	0.807	0.790	0.810	0.765	0.765	0.810	0.667–0.947
Resnet34 + Radiomics	0.806	0.763	1.000	0.500	1.000	0.690	0.667–0.944
Resnet50 + Radiomics	0.878	0.868	1.000	0.808	1.000	0.706	0.766–0.990
Resnet101 + Radiomics	0.801	0.790	0.750	0.818	0.818	0.750	0.657–0.946
Resnet152 + Radiomics	0.794	0.816	0.944	0.700	0.933	0.739	0.647–0.942
Densenet121 + Radiomics	0.778	0.816	0.727	0.852	0.885	0.667	0.617–0.938
EfficientNet + Radiomics	0.754	0.790	0.706	0.857	0.783	0.800	0.585–0.922
Inception + Radiomics	0.718	0.658	0.917	0.539	0.933	0.478	0.548–0.888

precise diagnosis of cervical LNM before surgery remains a pressing clinical issue that needs resolution. In our study, Resnet50 combining with the DL characteristics of radiomic features presents substantial potential for identifying OCLNM in OC and OP SCC preoperatively.

Radiomics refers to the comprehensive quantification of disease phenotypes by applying quantitative imaging features[24]. According to the hypothesis regarding radiomics, the genomic heterogeneity may translate to expression in a disease intra heterogeneity that can be assessed through imaging[41,42]. The radiogenomics analysis by Aerts *et al*.[43] revealed that a prognostic radiomic signature, which reflects intratumor heterogeneity, is associated with underlying gene expression patterns. As demonstrated in the present study, the multifeature radiomics signature effectively predicts OCLNM and prognosis of patients with early-stage OC and OP SCC, which also supports the hypothesis that the radiomics signature has the potential to capture disease intra heterogeneity in a noninvasive manner. Recently, radiomics is widely applied to preoperatively evaluate the status of lymph node in oral squamous cell carcinoma as a noninvasive method[27,44–46]. A previous research utilized radiomics derived from diffusion-weighted imaging (DWI) and apparent diffusion coefficient (ADC) maps to predict OCLNM in the early-stage oral tongue squamous cell carcinoma[44]. The research suggested that a radiomics approach could enhance the preoperative assessment of cervical node status. However, the research did not evaluate the result in a validation cohort. Tomita *et al*.[45] built a radiomics model through machine learning, using CT texture features, which outperformed three readers when tested on the validation cohort (AUC values of 0.820–0.930). However, the credibility of the study is somewhat limited due to the small sample size used. Wang *et al*.[46] constructed a multiomics nomogram that integrated MRI radiomics, ADC, and lymph node size to predict OCLNM. The model demonstrated commendable performance, with AUC values of 0.830 and 0.797 in the training and validation cohorts, respectively. A different study showcased that a radiomics model, built upon MRI images, exhibited an impressive diagnostic efficiency[27]. This was evident when the model was applied to both training (with an AUC value of 0.995) and testing groups (with an AUC value of 0.872). Nevertheless, the studies referenced above were conducted in single-center settings without external validation. Additionally, they primarily focused on traditional radiomics features derived from imaging.

Recently, DL as a novel method was widely applied in head and neck cancer imaging. A multitude of research has showcased the ability of DL algorithms to identify complex patterns in medical images, effectively adjust to new information, and achieve accuracy that matches or even surpasses human capabilities[28,47–50]. These algorithms have proven particularly effective in managing head and neck cancer by enabling personalized treatment plans and predicting outcomes[28,51,52]. In this study, we hypothesize that combining DLF with traditional radiomics features will provide a sanity check that DL radiomic models focus on regions within the images that are of importance for OCLNM. Compared with previous studies, we extracted DL features to explore the feasibility of applying a DL approach for distinguishing between LNM positive and LNM negative OC and OP SCC patients, and then combined DL features with traditional radiomic features to predict OCLNM. Among the 18 features screened in Resnet50 DL model, 13 were DLF, indicating that the DL technique may have extracted quantitative information reflecting OCLNM. In our research, we found that the Resnet50 DL model, which is based on both DL and radiomic features, outperformed the model based solely on radiomic features. This highlights the significant potential of the DL approach in predicting OCLNM. Furthermore, the Resnet50 DL model proves to be efficient in predicting the prognosis of the early OC and OP SCC patients. This further clarifies that the identified features can represent the tumor's heterogeneity, suggesting that our model holds promise for additional clinical applications.

To the best of our knowledge, this study is the first to apply the DL features and traditional radiomic features for predicting OCLNM. However, there are several limitations in this study. Firstly, this study was limited by its retrospective nature, a subsequently prospective study is needed to verify the capability of the proposed prediction model. Secondly, reliance on manual

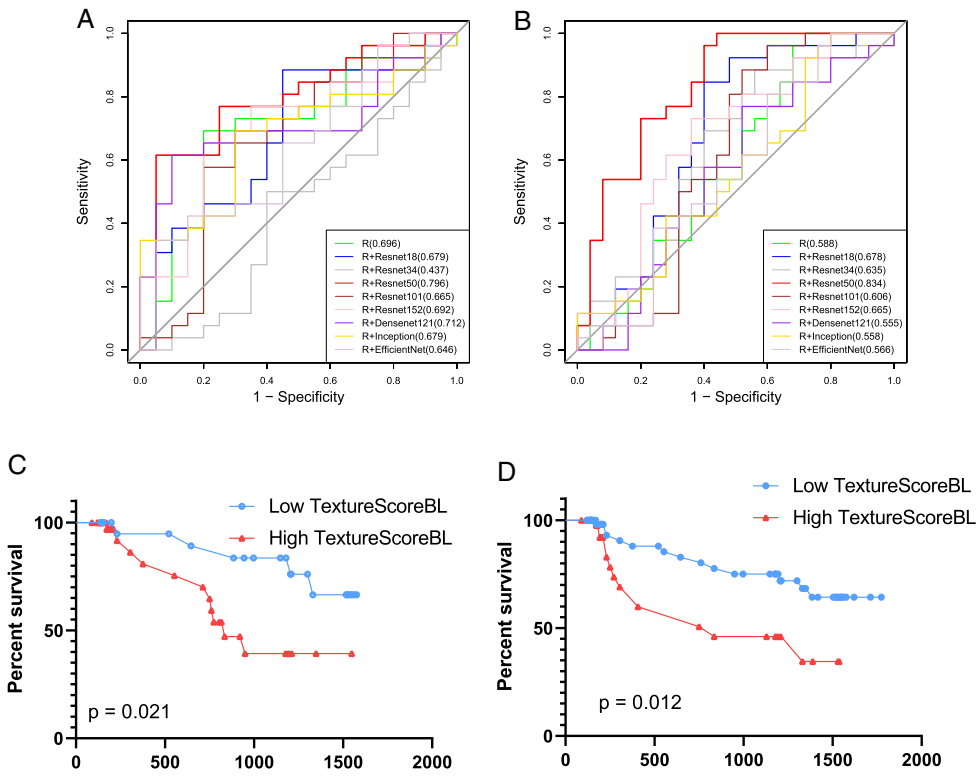

Figure 6. External validation of the of prediction models based on combined radiomics features and DLF. A. The ROC curve of prediction models based on combined radiomics features and DLF in the external validation set1; B. The ROC curve of prediction models based on combined radiomics features and DLF in the external validation set2; C. The Kaplan–Meier estimates of the Resnet50 model for predicting the overall survival rate of the patients in the external validation set1. D. The Kaplan–Meier estimates of the Resnet50 model for predicting the overall survival rate of the patients in the external validation set2.

Table 4

The external testing results of different DL methods in the external validation set1.

Experience	AUC	ACC	SPE	SEN	PPV	NPV	Delong (95% CI)
Radiomics	0.696	0.739	0.800	0.692	0.818	0.667	0.535–0.858
Radiomics + Resnet18	0.679	0.739	0.550	0.885	0.719	0.786	0.516–0.841
Radiomics + Resnet34	0.437	0.543	0.600	0.500	0.480	0.619	0.261–0.612
Radiomics + Resnet50	0.796	0.761	0.950	0.615	0.941	0.655	0.666–0.927
Radiomics + Resnet101	0.665	0.674	0.800	0.577	0.789	0.593	0.495–0.836
Radiomics + Resnet152	0.692	0.717	0.800	0.654	0.809	0.640	0.531–0.854
Radiomics + Densenet121	0.712	0.739	0.900	0.615	0.889	0.643	0.557–0.866
Radiomics + EfficientNet	0.646	0.609	0.950	0.346	0.900	0.528	0.485–0.807
Radiomics + Inception	0.679	0.696	0.700	0.692	0.750	0.636	0.522–0.836

Table 5

The external testing results of different DL methods in the external validation set2.

Experience	AUC	ACC	SPE	SEN	PPV	NPV	Delong (95% CI)
Radiomics	0.588	0.647	0.320	0.962	0.595	0.889	0.425–0.750
Radiomics + Resnet18	0.678	0.725	0.600	0.846	0.688	0.789	0.520–0.837
Radiomics + Resnet34	0.635	0.667	0.440	0.885	0.622	0.786	0.478–0.793
Radiomics + Resnet50	0.834	0.784	0.600	0.962	0.714	0.938	0.721–0.947
Radiomics + Resnet101	0.606	0.686	0.480	0.885	0.639	0.800	0.436–0.777
Radiomics + Resnet152	0.665	0.686	0.640	0.731	0.679	0.696	0.509–0.821
Radiomics + Densenet121	0.555	0.627	0.480	0.769	0.606	0.667	0.391–0.720
Radiomics + EfficientNet	0.566	0.608	0.400	0.808	0.667	0.583	0.588–0.869
Radiomics + Inception	0.558	0.608	0.280	0.923	0.778	0.571	0.508–0.764

tumor segmentation may introduce observer variability, underscoring the need for automated segmentation in subsequent research. Beyond these limitations, it is essential to highlight the transformative potential of artificial intelligence (AI) in refining clinical decision-making processes. Our predictive model, a confluence of AI and radiomics, presents a valuable tool for clinicians to make more informed decisions regarding the management and treatment of patients with OCLNM. Offering enhanced accuracy in predicting LNM, the model promises to guide the selection of optimal surgical and therapeutic interventions, thereby potentially elevating patient outcomes. Furthermore, the adoption of automated tumor segmentation in future investigations promises to optimize the clinical workflow by minimizing variability and augmenting the efficiency of diagnosis and treatment strategizing. In the future, several critical issues remain unaddressed, including noncompliance with machine learning best practices, standardization of radiomics workflows, and clinical adoption to fill the 'clinical transition gap' of the model. Addressing these challenges is crucial for maximizing the model's utility and impact in clinical settings.

Conclusion

In conclusion, DLF provide important information for prognosis of OCLNM in the early OC and OP SCC. The model based on combination of DLF and radiomic features could comprehensively assess OCLNM and prognosis of early OC and OP SCC and improve treatments for patients.

Ethical approval

This study was approved by the Ethics Committee of Hospital of Stomatology, Sun Yat-sen University (ERC-[2017]-30) and the Institutional Review Board of Sun Yat-sen Memorial Hospital, Sun Yat-sen University (No.SYSKY-2023-426-01).

Consent

This was a retrospective study, the ethics review passed the informed consent exemption, we protect the privacy rights of patients' and Patients' and volunteers' names, initials, or hospital numbers were not used.

Sources of funding

This work was supported by grants from the National Natural Science Foundation of China (Grant Nos. 81872194 U21A6005, 12226004); the Guangdong Science and Technology Development Fund (Grant Nos. 2017A030311011); Youth Project of Basic and Applied Basic Research Foundation of Guangdong Province (Grant Nos. 2021A1515110828) 2024 Basic and Applied Basic Research Project (Young Doctor "Sailing" project) of Guangzhou (Grant Nos. 2024A04J4948); the Guangdong Basic and Applied Basic Research Foundation (Grant Nos. 2023A1515110704).

Author contribution

T.J.L., S.J.K., P.S.L., and H.T.C.: conceived and designed the study; T.J.L., S.J.K., Q.X.L., L.S.W., J.T.L., X.H.D., L.J.Y., H.J. H., and J.K.L.: performed the data acquisition and analysis; T.J. L., P.S.L., C.L.N., Y.Y.L., H.C., X.S., Y.H., and F.W.: interpreted the results of this study; T.J.L., Y.Y.W., Z.Y.L., and S.J.K.: wrote the original manuscript; D.Z., C.L.N., and J.S.L.: reviewed and revised the manuscript. All authors contributed to this study and article, and approved the submitted version.

Conflicts of interest disclosure

The authors declare that there is no conflict of interest regarding the publication of this paper.

Research registration unique identifying number (UIN)

NCT06366906.

Guarantor

Haotian Cao and Jinsong Li.

Data availability statement

The datasets used and analyzed during the present study are available from the corresponding author on reasonable request.

Provenance and peer review

Not commissioned, externally peer-reviewed.

Acknowledgement

Assistance with the study: none.
Presentation: none.

References

[1] Nör JE, Gutkind JS. Head and neck cancer in the new era of precision medicine. J Dent Res 2018;97:601–2.
[2] Matos LL, Guimarães YLM, Leite AK, *et al*. Management of stage III oral cavity squamous cell carcinoma in light of the new staging system: a critical review. Curr Oncol Rep 2023;25:107–13.
[3] Gurmeet Singh A, Sathe P, Roy S, *et al*. Incidence and impact of skip metastasis in the neck in early oral cancer: reality or a myth? Oral Oncol 2022;135:106201.
[4] Keski-Santti H, Atula T, Tornwall J, *et al*. Elective neck treatment versus observation in patients with T1/T2 N0 squamous cell carcinoma of oral tongue. Oral Oncol 2006;42:96–101.
[5] Acevedo JR, Fero KE, Wilson B, *et al*. Cost-effectiveness analysis of elective neck dissection in patients with clinically node-negative oral cavity cancer. J Clin Oncol 2016;34:3886–91.
[6] Muhammad AY, Dhanani R, Salman S, *et al*. Depth of invasion as a predictor of cervical nodal metastasis of oral tongue squamous cell carcinoma: findings from a tertiary care center in Pakistan. Cureus 2021;13:e18976.
[7] Sakai T, Saito Y, Tateishi Y, *et al*. Tumor-stroma ratio can predict lymph-node metastasis in cT1/2N0 oral tongue squamous cell carcinoma independent of tumor budding grade. Int J Clin Oncol 2022;27:1818–27.
[8] Mamic M, Lucijanic M, Manojlovic L, *et al*. Prognostic significance of extranodal extension in oral cavity squamous cell carcinoma with occult neck metastases. Int J Oral Maxillofac Surg 2021;50:309–15.
[9] van Lanschot CGF, Klazen YP, de Ridder MAJ, *et al*. Depth of invasion in early stage oral cavity squamous cell carcinoma: the optimal cut-off value for elective neck dissection. Oral Oncol 2020;111:104940.

[10] Hori Y, Kubota A, Yokose T, *et al*. Prognostic role of tumor-infiltrating lymphocytes and tumor budding in early oral tongue carcinoma. Laryngoscope 2021;131:2512–8.
[11] Jang SS, Davis ME, Vera DR, *et al*. Role of sentinel lymph node biopsy for oral squamous cell carcinoma: current evidence and future challenges. Head Neck 2023;45:251–65.
[12] Yamazaki Y, Saitoh M, Notani K, *et al*. Assessment of cervical lymph node metastases using FDG-PET in patients with head and neck cancer. Ann Nucl Med 2008;22:177–84.
[13] Sun R, Tang X, Yang Y, *et al*. (18)FDG-PET/CT for the detection of regional nodal metastasis in patients with head and neck cancer: a meta-analysis. Oral Oncol 2015;51:314–20.
[14] Sumi M, Ohki M, Nakamura T. Comparison of sonography and CT for differentiating benign from malignant cervical lymph nodes in patients with squamous cell carcinoma of the head and neck. AJR Am J Roentgenol 2001;176:1019–24.
[15] Shin NY, Lee JH, Kang WJ, *et al*. Clinical usefulness of [18F]FDG PET-CT and CT/MRI for detecting nodal metastasis in patients with hypopharyngeal squamous cell carcinoma. Ann Surg Oncol 2015;22:994–9.
[16] Takamochi K, Yoshida J, Murakami K, *et al*. Pitfalls in lymph node staging with positron emission tomography in non-small cell lung cancer patients. Lung Cancer 2005;47:235–42.
[17] Lambin P, Rios-Velazquez E, Leijenaar R, *et al*. Radiomics: extracting more information from medical images using advanced feature analysis. Eur J Cancer 2012;48:441–6.
[18] Paul R, Hawkins SH, Schabath MB, *et al*. Predicting malignant nodules by fusing deep features with classical radiomics features. J Med Imaging (Bellingham) 2018;5:011021.
[19] Parekh V, Jacobs MA. Radiomics: a new application from established techniques. Expert Rev Precis Med Drug Dev 2016;1:207–26.
[20] Chakraborty J, Midya A, Gazit L, *et al*. CT radiomics to predict high-risk intraductal papillary mucinous neoplasms of the pancreas. Med Phys 2018;45:5019–29.
[21] Zwanenburg A. Radiomics in nuclear medicine: robustness, reproducibility, standardization, and how to avoid data analysis traps and replication crisis. Eur J Nucl Med Mol Imaging 2019;46:2638–55.
[22] Yip SSF, Aerts HJWL. Applications and limitations of radiomics. Phys Med Biol 2016;61:R150–166.
[23] Zwanenburg A, Vallières M, Abdalah MA, *et al*. The image biomarker standardization initiative: standardized quantitative radiomics for high-throughput image-based phenotyping. Radiology 2020;295:328–38.
[24] Gillies RJ, Kinahan PE, Hricak H. Radiomics: images are more than pictures, they are data. Radiology 2016;278:563–77.
[25] Illimoottil M, Ginat D. Recent advances in deep learning and medical imaging for head and neck cancer treatment: MRI, CT, and PET scans. Cancers (Basel) 2023;15.
[26] Esteva A, Kuprel B, Novoa RA, *et al*. Dermatologist-level classification of skin cancer with deep neural networks. Nature 2017;542:115–8.
[27] Wang F, Tan R, Feng K, *et al*. Magnetic resonance imaging-based radiomics features associated with depth of invasion predicted lymph node metastasis and prognosis in tongue cancer. J Magn Reson Imaging 2022;56:196–209.
[28] Huynh BN, Groendahl AR, Tomic O, *et al*. Head and neck cancer treatment outcome prediction: a comparison between machine learning with conventional radiomics features and deep learning radiomics. Front Med (Lausanne) 2023;10:1217037.
[29] von Elm E, Altman DG, Egger M, *et al*. The strengthening the reporting of observational studies in epidemiology (STROBE) statement: guidelines for reporting observational studies. Int J Surg 2014;12:1495–9.
[30] Bossuyt PM, Reitsma JB, Bruns DE, *et al*. STARD 2015: an updated list of essential items for reporting diagnostic accuracy studies. BMJ 2015;351:h5527.
[31] Alsharif U, Steller D, Falougy M, *et al*. The benefit of postoperative radiotherapy and extending neck dissection in pT1-2 oral squamous cell carcinoma with a single ipsilateral cervical lymph node metastasis (pN1). Anticancer Res 2022;42:97–104.
[32] Fan S, Tang Q, Lin Y, *et al*. A review of clinical and histological parameters associated with contralateral neck metastases in oral squamous cell carcinoma. Int J Oral Sci 2011;3:180–91.
[33] D'Cruz AK, Vaish R, Kapre N, *et al*. Elective versus therapeutic neck dissection in node-negative oral cancer. N Engl J Med 2015;373:521–9.
[34] Shen Z, Li J, Chen W, *et al*. The latest advancements in selective neck dissection for early stage oral squamous cell carcinoma. Curr Treat Options Oncol 2017;18:31.
[35] Matsubara R, Kawano S, Chikui T, *et al*. Clinical significance of combined assessment of the maximum standardized uptake value of F-18 FDG PET with nodal size in the diagnosis of cervical lymph node metastasis of oral squamous cell carcinoma. Acad Radiol 2012;19:708–17.
[36] Snow GB, Patel P, Leemans CR, *et al*. Management of cervical lymph nodes in patients with head and neck cancer. Eur Arch Otorhinolaryngol 1992;249:187–94.
[37] Jiang S, Locatello LG, Maggiore G, *et al*. Radiomics-based analysis in the prediction of occult lymph node metastases in patients with oral cancer: a systematic review. J Clin Med 2023;12.
[38] Park JT, Roh JL, Kim JS, *et al*. (18)F FDG PET/CT versus CT/MR Imaging and the prognostic value of contralateral neck metastases in patients with head and neck squamous cell carcinoma. Radiology 2016;279:481–91.
[39] Ng SH, Yen TC, Liao CT, *et al*. 18F-FDG PET and CT/MRI in oral cavity squamous cell carcinoma: a prospective study of 124 patients with histologic correlation. J Nucl Med 2005;46:1136–43.
[40] Huang SH, Hwang D, Lockwood G, *et al*. Predictive value of tumor thickness for cervical lymph-node involvement in squamous cell carcinoma of the oral cavity: a meta-analysis of reported studies. Cancer 2009;115:1489–97.
[41] Davnall F, Yip CSP, Ljungqvist G, *et al*. Assessment of tumor heterogeneity: an emerging imaging tool for clinical practice? Insights Imaging 2012;3:573–89.
[42] Diehn M, Nardini C, Wang DS, *et al*. Identification of noninvasive imaging surrogates for brain tumor gene-expression modules. Proc Natl Acad Sci U S A 2008;105:5213–8.
[43] Aerts HJWL, Velazquez ER, Leijenaar RTH, *et al*. Decoding tumour phenotype by noninvasive imaging using a quantitative radiomics approach. Nat Commun 2014;5:4006.
[44] Ren J, Yuan Y, Tao X. Histogram analysis of diffusion-weighted imaging and dynamic contrast-enhanced MRI for predicting occult lymph node metastasis in early-stage oral tongue squamous cell carcinoma. Eur Radiol 2022;32:2739–47.
[45] Tomita H, Yamashiro T, Heianna J, *et al*. Nodal-based radiomics analysis for identifying cervical lymph node metastasis at levels I and II in patients with oral squamous cell carcinoma using contrast-enhanced computed tomography. Eur Radiol 2021;31:7440–9.
[46] Wang Y, Yu T, Yang Z, *et al*. Radiomics based on magnetic resonance imaging for preoperative prediction of lymph node metastasis in head and neck cancer: machine learning study. Head Neck 2022;44:2786–95.
[47] Zhou Z, Chen L, Sher D, *et al*. Predicting lymph node metastasis in head and neck cancer by combining many-objective radiomics and 3-dimensioal convolutional neural network through evidential reasoning. Annu Int Conf IEEE Eng Med Biol Soc 2018;2018:1–4.
[48] Zhong YW, Jiang Y, Dong S, *et al*. Tumor radiomics signature for artificial neural network-assisted detection of neck metastasis in patient with tongue cancer. J Neuroradiol 2022;49:213–8.
[49] Kawamura K, Lee C, Yoshikawa T, *et al*. Prediction of cervical lymph node metastasis from immunostained specimens of tongue cancer using a multilayer perceptron neural network. Cancer Med 2023;12:5312–22.
[50] Song H, Yang S, Yu B, *et al*. CT-based deep learning radiomics nomogram for the prediction of pathological grade in bladder cancer: a multicenter study. Cancer Imaging 2023;23:89.
[51] Cheng NM, Yao J, Cai J, *et al*. Deep learning for fully automated prediction of overall survival in patients with oropharyngeal cancer using FDG-PET imaging. Clin Cancer Res 2021;27:3948–59.
[52] Wang Y, Lombardo E, Avanzo M, *et al*. Deep learning based time-to-event analysis with PET, CT and joint PET/CT for head and neck cancer prognosis. Comput Methods Programs Biomed 2022;222:106948.